RSC Advances

ROYAL SOCIETY OF CHEMISTRY

PAPER

View Article Online
View Journal | View Issue

Cite this: *RSC Adv.*, 2022, **12**, 27977

Controlled evaporation-induced phase separation of droplets containing nanogels and salt molecules†

Yuandu Hu *

Droplets without protection from surfactants or surfactant-like objects normally experience merging or a coalescence process since it is thermodynamically favored. However, division or replication of droplets is thermodynamically unfavored and comparably more difficult to realize. Herein, we demonstrate that a population of droplets that are composed of nanogels and salt spontaneously undergo a separation process under a slow solvent evaporation condition. Each individual droplet underwent changes in size, shape and eventually developed into two domains, which was caused by the screening effect due to the increased salt concentration as a result of solvent evaporation. The two domains gradually separated into nanogel-rich and salt-rich parts. These two parts eventually evolved into nanogel aggregates and branched structures, respectively. This separation was mainly due to the salting out effect and dewetting. Comparison studies indicate that both the nanogels and salt are indispensable ingredients for the phase separation. These discoveries may have profound applications in the fields of biomimetics and offer new routes for self-replication systems.

Received 23rd July 2022
Accepted 22nd September 2022

DOI: 10.1039/d2ra04585k

rsc.li/rsc-advances

1. Introduction

Droplets are self-organized structures where one liquid is dispersed in another surrounding liquid. The two liquids can be either immiscible or partially miscible.[1–3] Normally, a boundary exists between the two liquids and sometimes the boundary is stabilized by surfactants or surfactant-like lipids, polymers or even colloids.[4–8] The presence of these stabilizers could prevent droplets from undergoing coalescence.[9] The droplets are thermodynamically unstable and tend to merge without the protection from those stabilizers. Meanwhile, interfacial tension between the two liquids tends to force the droplets to display an energetically favorable configuration, such as being spherical in shape, which is similar to that of the protocells.[10] Throughout living systems in our universe, the fundamental behaviors of protocells is quite contrary to the abovementioned phenomenon of the droplets. Essentially, the most common and important feature of living systems is that the building blocks of these species, such as cells, could replicate and eventually lead to the growth in population, not only in terms of quantity, but also in volume. In the origin of life initiatives, a great amount of effort has been dedicated to explore the division of droplets, vesicles and other objects. Those attempts in objects' division could eventually result in the quantity growth of the objects, so as to mimic the behaviors of fundamental units of our living systems.[1,11–17] These approaches to realize an object's replication either require a rapid mass intake from ambient medium *via* a diffusion process or involvement of an external stimulus, such as a mechanical stimulus, chemical energy, electric field or other means.[18–23] The endeavors have been implemented both in theoretical and experimental studies.[1,24,25] Through those designs, the objects, such as droplets or capsule-like structures, start to undergo a switch in status from equilibrium to non-equilibrium, and further lead to changes in shape or eventually divisions.[26] As a result, the objects display a collective growth in quantity in the process. However, to date, spontaneous objects' growth in quantity has rarely been realized *via* a straightforward process, particularly a process without the need of feeding materials into objects or imposing an external stimulus on the objects. For example, DeSimone *et al.* reported spontaneous division and motility of an active droplet from the simulation point of view. This division and motility behavior was due to the interplay between active stresses and the defective geometry of the nematic director.[27] Chen, Lee, Keating and Shum *et al.* respectively reported the division-like behaviors of microobjects (*i.e.* droplets or vesicles) by leveraging mass exchange between the microobjects and an external medium.[4,11,28,29] All of the processes in those reports took place in a rapid fashion (normally within a matter of tens of seconds or a few minutes) and required mass-exchange. Microobjects' separation in a spontaneous and better controlled fashion have yet to be achieved. In this report, we demonstrate that water in oil (W/O) emulsion droplets could

Departments of Materials Science and Engineering, Department of Physics, School of Physical Science and Engineering, Beijing Jiaotong University, Beijing, China. E-mail: huyd@bjtu.edu.cn

† Electronic supplementary information (ESI) available. See https://doi.org/10.1039/d2ra04585k

show spontaneous phase separation through a controlled solvent evaporation process. The phase separation could lead to the object growth in a collective manner. The droplets are composed of two essential components: $Ru(bpy)_3$ moiety-functionalized nanogels, a certain amount of salts, such as Sodium Bromate ($NaBrO_3$) and initiator Potassium Persulfate (KPS) if necessary. The droplets dynamically change in size and shape, and subsequently evolve into two domains: nanogel-rich and salt-rich domains. Continued water loss leads to the two domains respectively developing into two separated parts: dumpling-like gel particle-based superstructures and highly branched crystal-like structures that are based on the hybridization of nanogels and salt molecules. The nanogel-based superstructures can be further immobilized upon gentle addition of tetramethyl ethylenediamine (TEMED) if KPS was premixed with the droplets' phase prior to the droplets' manufacturing process. It is found that each individual droplet in such a two-phase system could undergo a shape transformation and a subsequent asymmetric phase separation behavior, which enables the individual droplet to evolve into two or even multiple separated parts. This process takes place solely under the driven of solvent (water) evaporation and without any need of extra stimulus. Our discoveries have profound implications: on the one hand, this preliminary study may pave a way for the design and construction of artificial protocells and to study their evolutions for the origin of life community; on the other hand, this route also offers new opportunities for the design of unconventional soft or hybrid micro-objects and even their further applications in biomimetic, catalysis and pharmaceutics or other interdisciplinary areas.[30–33]

2. Experimental section

2.1 Materials

N-Isopropyl acrylamide (NIPAAm, ≥99%), *N*,*N*′-methylenebisacrylamide (BIS, 99%), potassium persulfate (KPS, ≥98%), sodium bromate ($NaBrO_3$, 99%), tris(2,2′-bipyridyl) dichlororuthenium(II) hexahydrate (99.95%), acrylic acid (AAc, 98%), 1-decanol (99%), methanol (anhydrous, >99.8%), 2-hydroxyethyl methacrylate (HEMA, 98%), 1-ethyl-3-(3-dimethyl aminopropyl) carbodiimide (EDC), sorbitan monooleate (Span 80), *N*,*N*,*N*′,*N*′-tetramethyl ethylenediamine (TEMED, ≥99.5%) and 2,2′-azobis(2-methyl propionitrile) (AIBN, 98%) were all from Sigma-Aldrich. 4-Vinyl-4′-methyl-2,2′-bipyridine (99%) was ordered from Ark Pharm, Inc. Ruthenium(II) (4-vinyl-4′-methyl-2,2′-bipyridine) bis(2,2′-bipyridine) bis(hexafluoro phosphate) (noted $Ru(bpy)_3$ monomer as below) was synthesized according to the previous literature with minor modifications.[34–39] All chemicals were used as received. Double distilled water was ordered from WaterLab Solutions and was a reverse osmosis product according to the information from the vendor.

2.2 Synthesis of ruthenium and acrylic acid dual-functionalized gel particles

Synthesis of the dual-functionalized gel particles was achieved using emulsification polymerization method based on previously report with modifications.[40] Briefly, NIPAAm (2.308 g, 22.1 mmol), BIS (0.172 g, 0.34 mmol), SDS (0.068 g, 0.24 mmol), acrylic acid (400 μL) and $Ru(bpy)_3$ monomer (0.17 g, 0.19 mmol) were dissolved in 70 mL of distilled water. To remove any possible granules, a 0.45 μm pore-size filter was used to filter the solution and after that, the solution was transferred into a 250 mL three-neck flask. The solution was degassed under nitrogen for at least 30 minutes. The flask was then heated to 70 °C with N_2 protection. 10 mL of KPS (0.069 g, 0.07 mmol) solution was added to the flask to initiate polymerization once the temperature was stabilized at 70 °C. The reaction was continued for another 6 hours under the same temperature and N_2 protection. The flask was immediately cooled down with an ice bath after the reaction. For purification, a stainless-steel mesh with a pore size of 15 μm was applied to filter out any larger aggregates. Then, the filtered gel particle solution was dialyzed against pure water for one week with frequent water change.

2.3 Modification of the pNIPAAm-AAc-$Ru(bpy)_3$ gel particles with HEMA

The purified pNIPAAm-*co*-AAc-*co*-$Ru(bpy)_3$ gel particles were further functionalized with HEMA to render gel particles with multiple vinyl groups. The modification route was based on previous reports.[41,42] Generally, 60 mL of the purified pNIPAAm-AAc-$Ru(bpy)_3$ gel particles solution was put into a 100 mL flat bottom flask. The flask was placed in an ice bath for 30 minutes and subsequently 2.8 g of HEMA was added into the flask. After another half hour of stirring and reaction in an ice bath, 2.1 g of EDC in 5 mL water was added to the flask. The stirred reaction was maintained under the ice bath condition for another 3 hours. After the reaction, the collected product was dialyzed against pure water for one week with frequent water change. The purified product was freeze-dried. The obtained product was stored in a refrigerator for further use. To characterize the pNIPAAm-AAc-$Ru(bpy)_3$ and HEMA-modified pNIPAAm-AAc-$Ru(bpy)_3$ gel particles, d^6-DMSO was used as the solvent for both characterizations. ^{1}H NMR measurement was conducted on Bruker NMR spectroscopy (Inova500B (I500B)).

2.4 Preparation, purification and characterization of the colloid-based superstructures

Preparation of the superstructures was achieved through the spontaneous evaporation of water-in-oil (W/O) emulsions, which were fabricated *via* hand shaking and microfluidics approach, respectively. 1-Decanol solution of Span 80 was used as the oil phase. A mixture of aqueous solution of HEMA-modified pNIPAAm-AAc-$Ru(bpy)_3$ gel particles (3 wt%, 500 μL), aqueous solution of $NaBrO_3$ (2 M, 50 μL) and aqueous solution of KPS (1 wt%, 83 μL) was used as the dispersed water phase. A glass capillary-based microfluidic device was constructed according to previous report and used for the fabrication of emulsion droplets.[5,43] The orifices of injection tubing and collecting tubing are 160 μm and 520 μm, respectively. For droplets with different diameters, the flow rates of the dispersed phase varied from 100 to 1500 μL h^{-1} while the flow rate of the continuous phase was fixed at 4 mL h^{-1}. The droplets were then

collected in plastic Petri dishes (BIPEE polystyrene Petri dish 35 × 10 mm) unless specially noted and the sample was covered with a clean Petri dish cover to slow down the evaporation. For slow evaporation experiments, the samples were collected in plastic Petri dishes with another size (diameter × height 50 × 9 mm with a tight fit lid). The evolution of the samples in the Petri dishes was monitored under optical microscopy (AmScope IN300TC Long Working Distance Inverted Trinocular Microscope equipped with a PixeLink Colour Camera). The evolution of droplets was recorded using a Pixelink camera. Zeiss microscope (Axio Observer A1 Zeiss, Germany) was used for the fluorescence microscopy characterizations. The microscope was equipped with a camera and the fluorescence signal was irradiated by blue light (λ = 470 nm, 6.65 mW). For bulk emulsification, 200 μL aqueous solution of HEMA-modified gel particles was mixed with 30 μL of 1 wt% of KPS solution and the mixed aqueous solution was dispersed into 1 mL 1-decanol solution of Span 80 (5 wt%) *via* handshaking for 10 seconds. All the optical/fluorescence microscopy observation experiments were performed at 23.5 ± 0.5 °C.

2.5 Interfacial tension measurement

The interfacial tension measurements were performed on a home-made setup, which consists of a digital camera (to capture the image of droplets), a liquid cell and a syringe with a blunt needle to finely tune the size of droplets. The acquired images were subsequently processed by MATLAB program to calculate the interfacial tensions.

2.6 Dynamic light scattering (DLS) characterizations

0.1 wt% of aqueous dispersion of HEMA-modified gel particles was used as the DLS measurement sample. The gel particle dispersion was further characterized under a dynamic light scattering (DLS) machine (Delsa Nano Submicron Particle Size and Zeta Potential, Beckman-Coulter). A refractive index value of 1.3331 at 25 °C was used for H_2O. Given that the concentration of gel particles is low, it is supposed that there are no gel particle interactions. The size measurement was carried out at 23.5 °C. The light scattering angle was chosen as 90°. Cumulative size distribution results were adapted for analysis of size distribution.

3. Results and discussion

An aqueous phase that was composed of (hydroxyethyl) methacrylate (HEMA)-modified poly(*N*-isopropyl acrylamide)-*co*-(acrylic acid)-*co*-(Ru(bpy)$_3$) (note as HEMA-*m*-pNIPAAm-*co*-AAc-*co*-Ru(bpy)$_3$) nanogels, $NaBrO_3$ and potassium persulfate (KPS), and an oil phase of Span 80 in 1-decanol solution were used as dispersed phase and continuous phase, respectively. The addition of Span 80 in the oil phase assists to prevent droplets from undergoing coalescence. By using appropriate emulsification method, water in oil (W/O) emulsion droplets can be obtained. The droplets preparation process in the present study was mainly achieved through microfluidics so as to obtain droplets with uniform size, despite handshaking method was also utilized to test the generality of the droplet behaviors. The HEMA groups and Ru(bpy)$_3$ moieties in the nanogels respectively provide gel particles with further intercross linking capability (due to the introduction of multiple vinyl groups) and facile tracking property (due to the orange color and different refractive index). The synthetic routes and chemical structures of gel particles are shown in Fig. S1† and 1. Fig. S2 and S3† show the ^{1}H NMR characterizations of the nanogels. The appearance of peaks at 5.6 ppm and 6.0 ppm after HEMA modifications indicates that the successful introduction of vinyl groups onto the backbone of the gel particles. Fig. S4† shows the dynamic light scattering (DLS) results of the HEMA-modified gel particles in pure water solution. The nanogels have an average hydrodynamic diameter of ~235 nm with a PDI (polydisperse index) of ~0.15. Fig. 1(a) shows the droplets generation process inside a glass capillary based microfluidic apparatus, which has been widely used for droplets preparation in many other reports.[43–46] Fig. 1(b) shows the droplets just after collection and displaying uniform size. The droplets settled at the bottom of the container due to their higher density (~1 g cm^{-3}) than that of the surrounding decanol medium (~0.83 g cm^{-3}). Fig. 1(c) illustrates the composition of the nanogel-containing droplets and the schematic structure of the gel particles. Fig. 1(d) depicts the chemical structure of the gel particles.

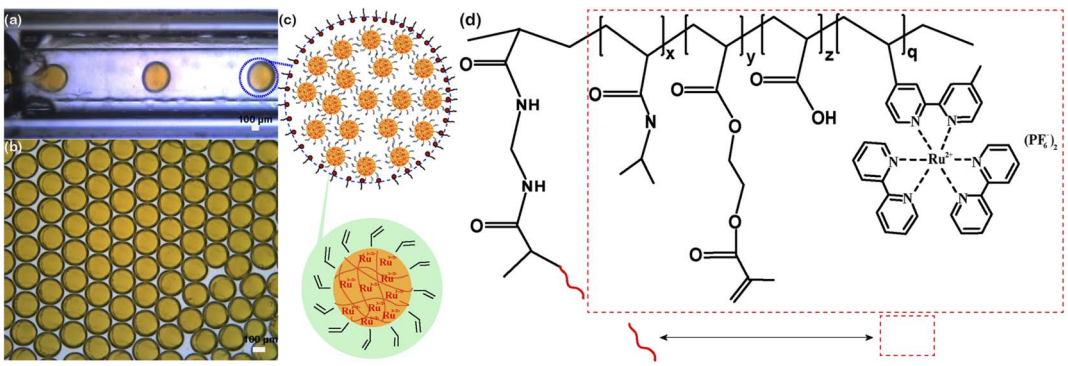

Fig. 1 (a) Optical microscopy image of the process of generating nanogel-containing droplets inside the microfluidic device; (b) optical microscopy image of the collected droplets in a transparent plastic Petri dish; (c) illustration figures of the nanogel-containing droplets and the nanogels; (d) chemical structure of the nanogels.

3.1 Evolution of droplets containing both gel particles and salt molecules

Scientists in the origin of life community have been actively searching for systems that could achieve the self-replication process, which can consequently induce the growth of population and eventually thrive civilization. Here we demonstrate how our gel particle-containing droplets spontaneously undergo a phase separation process, which may have

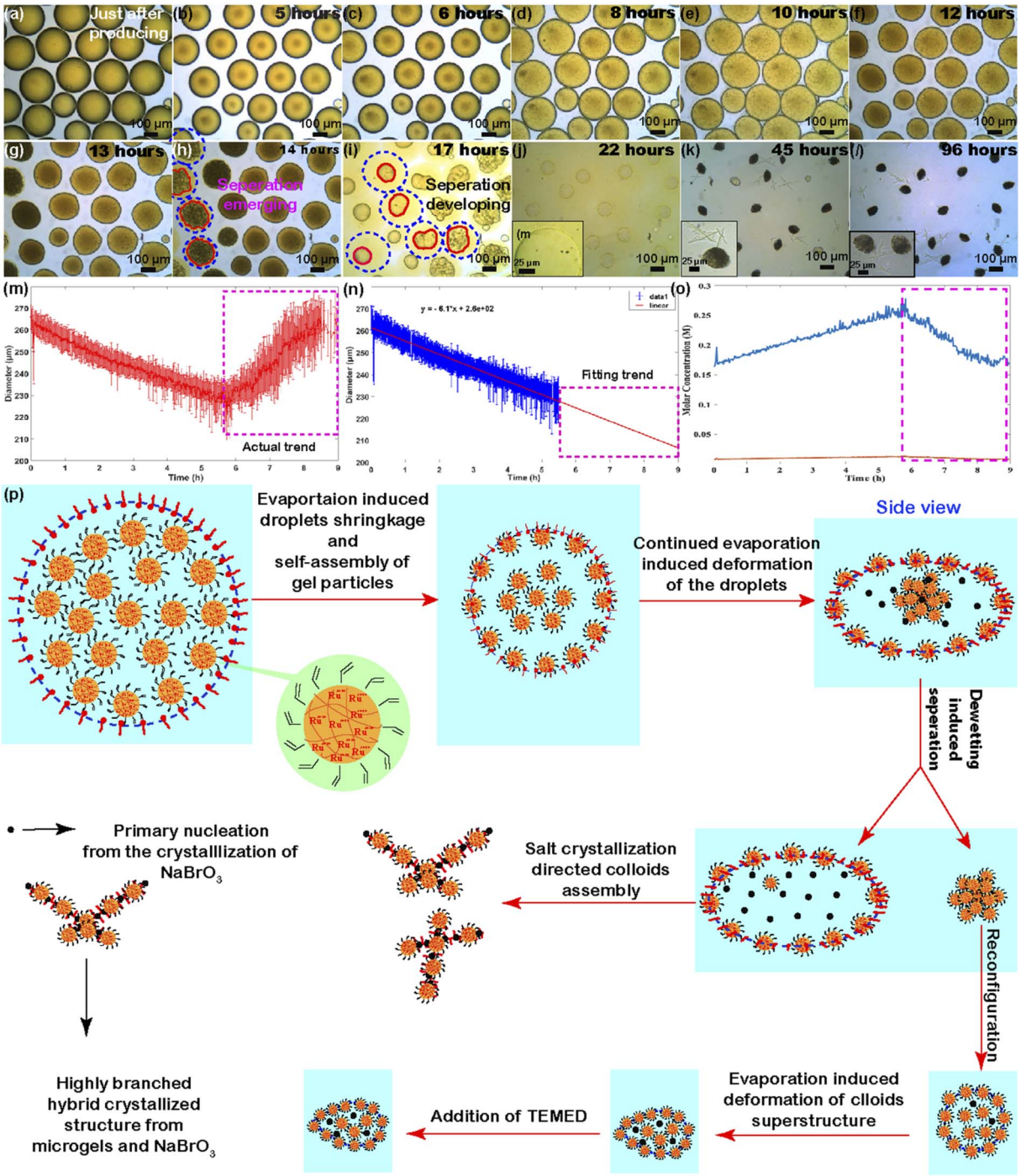

Fig. 2 (a–l) Optical microscopy images of the droplets containing gel particles and salt molecules evolved solely under the influence of solvent evaporation ($T = 23.3 \pm 0.5$ °C). (m) Diameter change of the droplets as a function of time. The dot-line square region shows the measured diameter change of the droplets when the droplets started flatten phase. (n) Fitted plot of the diameter change of the droplets as a function of time. The dot-line square region shows the fitted diameter change of the droplets when the droplets started flatten phase. (o) The molar concentrations of $NaBrO_3$(blue curve) and KPS (orange curve that is close to the x axis) change as a function of time during the evaporation process. The molar concentration changes were calculated based on the diameter measurement change in the plot (m). The dot-line square on the right side indicated that the concentration changes were no longer the actual concentration changes inside the droplets. (p) Illustration figure shows the evolution of the droplets containing gel particles and salt molecules.

potentially implications for further exploring this fundamental puzzle within the origin of life community. The nanogel-containing droplets began to evaporate once being collected in a container. Fig. 2 shows optical microscopy images of a population of the droplets evolving in a Petri dish. The droplets contained homogeneously distributed nanogels (the homogeneous fluorescence signal intensity in the Fig. S5† indicates that there is no microscopic visible nanogel aggregates) and firstly displayed a decrease in size, from ~270 μm to ~230 μm (as shown in Fig. 2a–c), which was due to the evaporation of solvent (water in our case) at room temperature in the droplets. As the evaporation proceeds, at some point (depends on the size of droplets), it looks like that the droplets display an increase in diameter (as shown in Fig. 2d–e and the right part of the curve in Fig. 2m). However, this trend does not reflect the actual scenario of what the droplets have experienced, but rather likely due to a shape transition of the droplets, specifically droplets' morphology transformed from spherical to oblate (termed as flatten process here).[47–50] This shape-transition process was likely caused by the formation of nanogel gradients within the individual droplets (from the bottom to the top part) under the effect of water evaporation. This nanogel particle ingredient inside individual droplet resulted in an interfacial tension ingredient, which together with the gravity to result in the deformation of the droplets.[50] Consequently, the oblate droplets displayed larger in diameter than their actual diameters when being observed from the top view of the microscopy observation.[51] Fig. 2f–g show the droplets displaying a size decrease trend again due to the diminishing of interfacial tension ingredient as the evaporation process continues (also shown in the Fig. S6 in ESI and Supporting Video 1†). Despite the actual size change of the droplets can't be directly determined from the optical microscopy images, the real size evolution trend for this period could be fitted and projected since the evaporation rate of droplets in this size range is constant (as shown in Fig. 2n).[52] Meanwhile, accompanied with the diameter change, the salts' concentration change as a function of time in the droplets can be also calculated for the evolution period prior to the droplets' flatten taking place. Fig. 2o shows the concentrations of $NaBrO_3$ (blue curve) and KPS (orange curve) change as a function of time. The concentrations of $NaBrO_3$ and KPS increased from an initial value at ~0.155 M and ~0.008 M to a peak value at ~0.25 M and 0.012 M prior to the droplets' flatten phase, respectively. The concentration of KPS is negligible when compared with that of $NaBrO_3$. After reaching the peak values, both concentration changes displayed a decrease trend (as shown in dot-line square part in Fig. 2o), which doesn't reflect the real concentration change. An interesting phenomenon, the separation of the droplets emerged when the evaporation process proceeds into a specific stage and this phase separation process gradually passed onto adjacent droplets, and further advanced to the entire population of the droplet sample (as indicated in Fig. 2h–i and Supporting Videos 1 and 2†). Assuming the phase separation of the droplets in Fig. 2 happened at 14 hours of observation, the droplets average diameter was around 186 μm according to the fitted curve in Fig. 2n, then the final concentration of salt just prior to phase separation was about 0.474 M. Typically, the phase separation process led to the spontaneous evolving of each individual droplet into two separate parts: nanogel-rich part (with relatively more intense orange color from the $Ru(bpy)_3$-functionalized nanogels) and salt-rich part (further confirmed by Fig. S7 and S8 in ESI,† where droplets were prepared by handshaking method and with relatively smaller diameters and each droplet after evolving displayed a fluorescence intense domain and less fluorescence domain). It is worth mentioning that droplets with wide size distributions in Fig. S7 and S8† also showed a similar transition process as that of the droplets with uniform size distribution. This phenomenon indicated that the droplets evolution process was independent of their initial sizes and size distributions in our observation range (note: there may be a size range that allow the droplets for experiencing the phase separation. The lower limit of the droplets' diameter could be smaller than 50 μm. However, I am not sure the upper limit of the droplets' diameter for allowing such kind of phase separation, given that the diameters of droplets were all below ~500 μm in our studies. We will figure out the threshold in our future investigations). This is different from phase separation phenomenon in some other droplet system.[28] The evolution of the two separated parts then followed two completely different pathways upon the continued evaporation of water. On the one hand, despite the gel particle-rich part underwent a shape deformation, the deformed structures gradually recovered to a spherical shape (gel particles' aggregate) due to the minimization of interfacial energy and self-organizing of the gel particles (as can be seen in ESI Video 1 and also in Video 2† when another batch of droplets were under relatively slow evaporation mode). The gel particle-rich part with spherical shape continued to evolve into deformed colloids-based superstructures due to the continued water loss (as shown in Fig. 2i–j and another batch of droplets' experiment in Fig. S9 in ESI†). On the other hand, the salt-rich part with relatively brighter contrast gradually faded with their spherical outline as well as the orange color, and eventually formed crystal like structures. This phenomenon was mainly due to the evaporation of water in the salt-rich domain, which consequently induced the crystallization of salt molecules, specifically $NaBrO_3$ molecules and tiny amount of KPS (as shown in Fig. 2k–l and also confirmed in another two batches of droplets' experiments in Fig. S6 and S9 in ESI†). Given that the salt-rich domain contained a large portion of salt molecules, the resulting structures of the salt-rich domain was completely dominated by the salt crystallization guided structure formation. Fig. 2p depicts the entire evolution of the droplets upon the influence of water evaporation.

Although the above-mentioned droplets mainly displayed a process that evolved from one individual droplet to two separate parts, we were also aware of another type of droplet evolution process: an individual mother droplet (the droplets directly produced from microfluidics) evolved from one integrity to multiple daughter parts (more than two different parts, namely one-to-multiple separation process, as shown in Fig. S10 in ESI and Video 3†), pretty like the continued developing of a budding process.[53] Unlike the droplets showed

one-to-two separation behavior, the one-to-multiple separation process only took place in the context of droplets containing a relatively higher amount of salts (however, at this moment it is not clear the exact threshold value of the salt concentration in the droplets that could trigger the one-to-multiple separation, but we will figure it out in our future studies).

To compare whether the evaporation velocity affects the droplets' evolution process, we also carried out experiments that the droplets were evolved under a slow solvent evaporation condition (as shown in Fig. S11 in ESI and Supporting Video 2†). The droplets evolution processes took place slightly less than two weeks and displayed a clear phase separation phenomenon, indicating that the occurrence of the phase separation process is prone to take place under slow solvent evaporation condition. In addition, we carried out experiments when the initial droplets with deformed shapes, which means that the droplets were not spherical in shape. The droplets in this case still displayed clear phase separation phenomenon (as shown in Fig. S12 in ESI and Supporting Video 4†).[54] This phenomenon indicates that the occurrence of phase separation is independent of the initial shapes of the droplets.

3.2 Evolution of droplets only containing gel particles or salt molecules

To explore which components inside the droplets played the key role to ensure the occurrence of phase separation phenomenon, we carried out experiments where the droplets only containing gel particles or only containing salt molecules. Fig. 3 shows a group of droplets only containing gel particles and evolving solely under the influence of solvent evaporation. The droplets in this case didn't show any phase separation phenomenon, but rather a pure drying process, ending up with dried orange residues (also as shown in Supporting Video 5†). Similarly, when the droplets only containing gels particles and evolved in a slow evaporation mode (where the evolution process lasted slightly less than two weeks), the droplets still didn't show any scenario of phase separation phenomena (as shown in Fig. S13†). In addition, when the droplets only contained salt molecules, they only experienced a pure solvent evaporation and drying process (as shown in Fig. S14 in ESI and Supporting Video 6†). These phenomena indicated that both the gel particles and salt ($NaBrO_3$ or $NaBrO_3$ and KPS combined) are essential ingredients to ensure the droplets to successful experience the phase separation process.

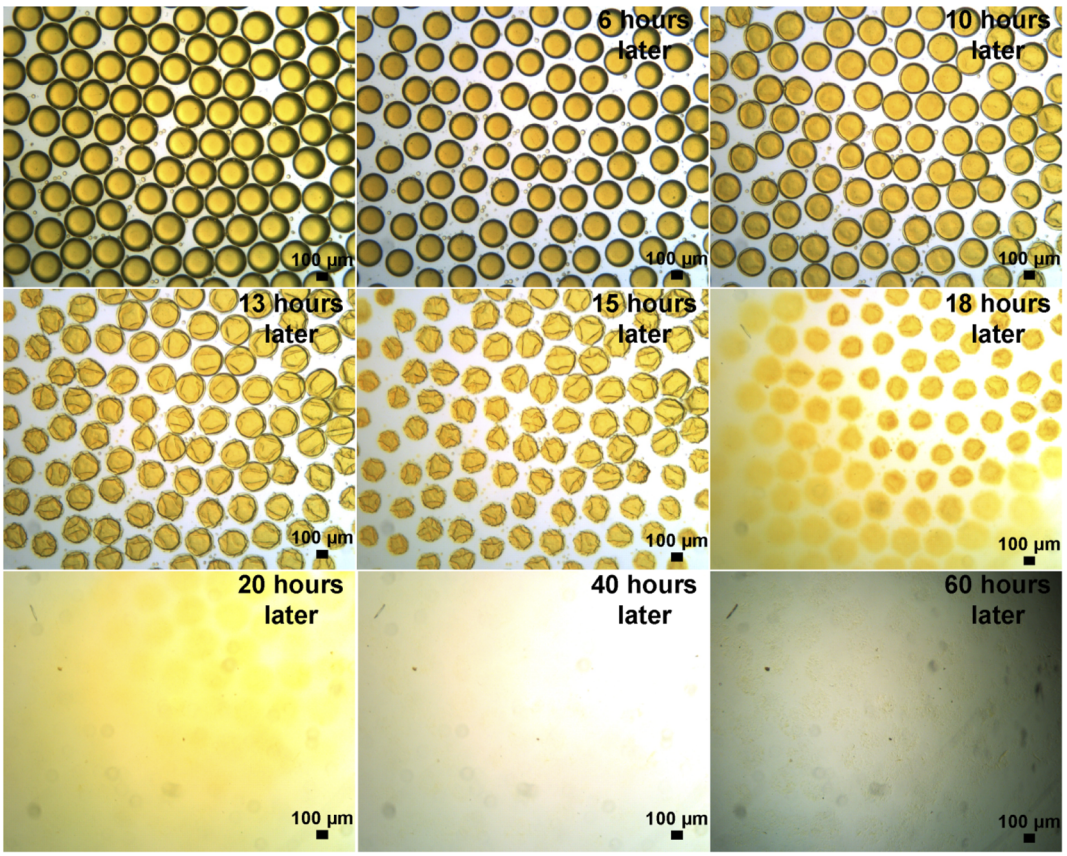

Fig. 3 Microscopy images of gel particles-containing droplets free of $NaBrO_3$ evolved at ~23.3 ± 0.5 °C. The droplets were in 1-decanol solution of Span 80 (the droplets' transformation process took place within 20 hours). It is clear that the droplets free of $NaBrO_3$ didn't show any separation phenomenon. Unlike the evolution of droplets containing both gel particles and $NaBrO_3$, the evolution of these salt-free droplets ended up with an almost blank background (with very small amount of orange gel particle residues), indicating that the presence of salt ($NaBrO_3$) played an essential role for the occurrence of phase separation.

3.3 Explore the underlying mechanism behind the droplets' evolution

To further explore and understand this process, we need to get a deep insight to the mechanisms behind those series of phenomena. At the very beginning, when the droplets were just produced from the microfluidic device and immediately collected in the container, the droplets system was considered as a two phases system: an oil phase (Span-80 in 1-decanol solution) and an aqueous phase (aqueous solution of nanogels and salts). The gel particles were homogeneously distributed inside the droplets due to the repulsive forces among nanogels (as confirmed by fluorescence microscopy images in Fig. S5,† where there were no notable nanogel aggregations under the fluorescence microscope). However, as water evaporation and the evolution of droplets emerged, the two phases system gradually transformed into three parts: the continuous oil phase, nanogel-rich phase (predominately by the aqueous solution of HEMA-modified pNIPAAm-AAc-Ru(bpy)$_3$ gel particles) and salt-rich phase (predominately by the aqueous solution of salt). Particularly, the droplets with homogeneously distributed gel particles gradually evolved into two separate parts: nanogel-rich part and salt-rich part. This transition was plausibly caused by the redistribution of gel particles under the driven of solvent evaporation. Solvent evaporation results in the concentration increases of each component in the droplets. Specifically, the increased salt concentration could lead to counteraction of repulsive force among nanogels.[55–57] And consequently, the nanogels start to aggregate. As the evaporation continues, gel particle aggregates gradually developed due to screening effect and moved towards the water/oil interface due to their amphiphilic properties. A direct consequence of this development eventually leads to the flocculation of gel particles. As the gel particles aggregation approached to a critical point, the gel particle-rich domain and salt-rich domain began to emerge. It is not difficult to image that the salt-rich domain and gel particle-rich domain get denser and lighter, respectively. So, the screening effect, gravity force on the salt-rich domain and buoyancy force on the gel particle-rich domain could synergically advance the evolving of the two domains. Meanwhile, the electrostatic repulsive force between gel particles gradually decreased due to the increased screening effect as the evaporation proceeds. According to the DLVO theory, the van der Waals force among gel particles also gradually became the dominant force and further advanced aggregation of gel particles.[58] The development of the two domains put the droplets to an extreme situation, where the separation

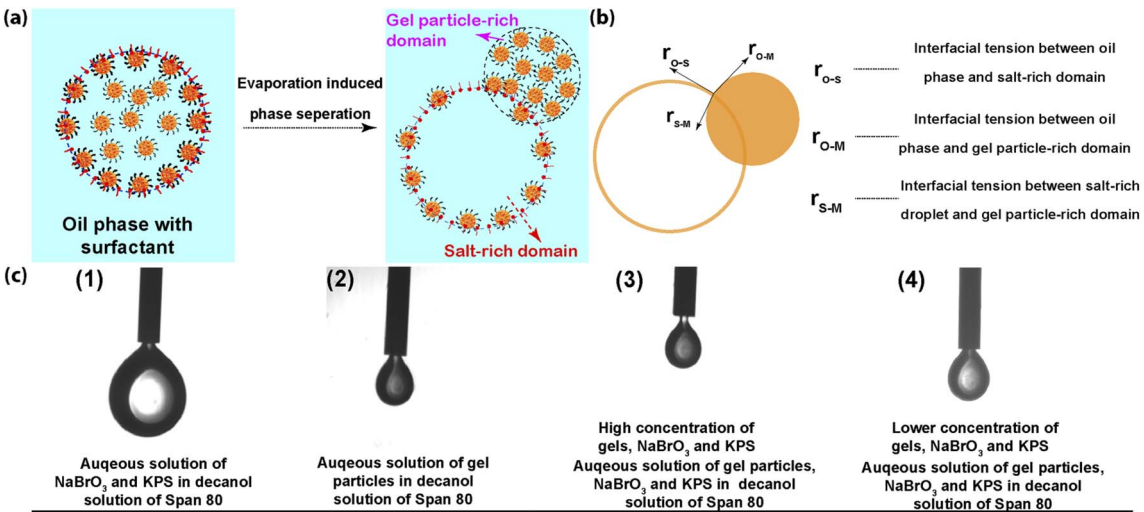

Number		(1)	(2)	(3)	(4)
Outer Oil Phase		5 wt% Span 80 in decanol	5 wt% Span 80 in decanol	5 wt% Span 80 in decanol	5 wt% Span 80 in decanol
Droplet Composition	3 wt% gel particle solution (μL)	0	500	500	500
	2 M $NaBrO_3$ solution (μL)	50	0	50	50
	1 wt% KPS solution (μL)	83	0	83	83
	H_2O (μL)	500	0	0	175
Density difference between the aqueous droplet and oil phase		0.194	0.154	0.186	0.182
Interfacial Tension (mN/m)		3.7	1.6	1.5	1.8

Fig. 4 (a) Illustration figure shows the droplet-shifting from a droplet with homogeneously distributed gel particles inside to an object composing two domains: gel particle-rich domain and salt-rich domain. (b) Illustration figure shows three different interfacial tensions among the external medium, gel particle-rich domain and salt-rich domain. (c) Interfacial tension measurements of droplets with different compositions and their corresponding values. The table at the bottom part is the compositions of droplets and their corresponding interfacial tensions.

phenomenon starts to emerge. Despite multiple factors, such as salt-out effect and buoyance force, may play roles at this stage, the dominate factor is supposed to be the wetting-to-dewetting transition of the droplets. This transition can be interpreted from the point view of the spreading parameters between different phases, as shown in Fig. 4. Basically, there were one and three interfaces before and after the emergence of the phase separation, respectively. Before the phase separation process, the sole interface was the one between the droplet and the oil phase. The corresponding interfacial tension is denoted as γ_{o-w}. Whilst at the moment of the emergence of phase separation, the number of interfaces increased from one to three, which were the interfaces: between oil phase and the gel particle-rich phase (o–m), between oil phase and the salt-rich phase and between the salt-rich phase and the gel particle-rich phase (s–m), respectively. The corresponding interfacial tensions were γ_{o-m}, γ_{o-s} and γ_{s-m}, respectively. Before and after the phase separation process, the gel particle-rich phase can be considered as completely wetted and partially dewetted by the salt-rich phase, respectively. Therefore, the spreading parameter can be expressed as eqn (1):

$$S = \gamma_{o-s} - \gamma_{s-m} - \gamma_{o-m} \quad (1)$$

To ensure the droplets successfully undergo a phase separation process, it is required that the $S < 0$.[59,60] At the moment of the phase separation began to emerge, the interfacial tensions can be measured since the concentrations of gel particles in the gel particle-rich phase and salt-rich phase can be fitted and determined from the curve. Despite the interface tension γ_{m-s} between the gel particle-rich phase and the salt-rich phase can't be measured directly since they are both miscible aqueous solutions, the value is normally in the range of 0.01–10 μN m^{-1} (1×10^{-4} to 10^{-2} mN m^{-1}) according to previous reports.[61,62] The interface tension between droplets with relatively higher amount of gel particles and oil phase (γ_{o-m}) and the interfacial tension between droplet with relatively higher amount of salt (γ_{o-s}) are 1.6 mN m^{-1} and 1.5 mN m^{-1}, respectively (as shown in Fig. 4c). Assuming the interfacial tension between the salt-rich phase and gel particle-rich phase is the minimum value of 10^{-4} mN m^{-1}. The value of the spreading parameter $S = 1.5–1.6–10^{-4} \approx -0.1$ mN m^{-1}, which indicated the dewetting phenomenon can be spontaneously triggered after a certain period of evaporation process, just like what we have observed in our experiments. As the water evaporation process proceeds, the γ_{o-s} would incrementally increase and therefore resulted in the S value moving towards a more negative direction (as shown in Fig. 4c(1) in the case of gel particle-free droplet). This move would further advance the phase separation process. This droplets' system may have important implications in the realms of self-replication systems and probably can be extended to some other applications as well.

4. Conclusions

In this study, we have successfully demonstrated a controlled evaporation-induced phase separation behavior of droplets system. Aqueous solution of droplets containing nanogels and small molecules (such as $NaBrO_3$ or $K_2S_2O_8$) were prepared by two different methods: microfluidic technique and handshaking approach, so as to produce droplets with uniform and polydisperse sizes for comparison study. Upon solvent (water) evaporation, the droplets can undergo a phase separation process that induced the evolution of each individual droplet into two separate parts: gel particle-rich part and salt-rich part. Further systematical study reveals that the initial droplets experienced a consecutive procedure: size decrease, shape flatten, two domains emerging and phase separation. These phenomena are likely due to the screening effect caused by the evaporation-induced salt concentration and consequently induces a phase separation due to the salt-out and dewetting effects. The initial droplets eventually evolve into two separate parts when the dewetting process proceeds. Comparison experiments indicate that the simultaneous presence of salt and gel particles plays an essential and critical role for the emergence of this phenomenon. The phase separation process is prone to take place under slow solvent evaporation condition and independent of initial droplet shapes and droplet sizes in our experimental observation range. After the phase separation process, the gel particle-rich part evolved into objects with different shapes, which have potential applications in the field of preparation of gel particle-based superstructures with different morphologies, specifically preparation of superstructures in an energy input-free manner rather than previously reported heating-cooling method.[63,64] The regulation of nanogel based superstructures *via* this evaporation approach will be our future research emphasis.[65] In addition, the phase separation process has profound implications for future studies in the fields of design biomimetic self-replication systems. The current study perhaps lays out a possible explanation for the emergence of protocells replication on earth.

Conflicts of interest

The authors declare no competing financial interest.

Acknowledgements

The majority of the experiments were carried out at Dr Juan Pérez-Mercader's laboratory in Harvard University. Dr Yuandu Hu is grateful for Dr Juan Pérez-Mercader's support and mentoring. Dr Yuandu Hu also thank Dr Alec Pawling for his assistance with the tracking the size change of the nanogel particle-containing droplets. This work was funded by Repsol, S. A., Spain and partially supported by Beijing Jiaotong University. The funders had no role in the study design, data collection and analysis, decision to publish, or preparation of the manuscript. NMR characterization was conducted at the Chemistry and Chemical Biology Department of Harvard University. DLS characterizations were performed in the Center for Nanoscale Systems (CNS) at Harvard University. We thank Mrs Anqi Chen for her assistance with interfacial tension measurements. Dr Yuandu Hu is grateful for the talent fund support from Beijing Jiaotong University under the grant number KSRC21006532.

References

1 D. Zwicker, R. Seyboldt, C. A. Weber, A. A. Hyman and F. Jülicher, *Nat. Phys.*, 2016, **13**, 408–413.
2 Z. Yang, J. Wei, Y. I. Sobolev and B. A. Grzybowski, *Nature*, 2018, **553**, 313–318.
3 D. C. Dewey, C. A. Strulson, D. N. Cacace, P. C. Bevilacqua and C. D. Keating, *Nat. Commun.*, 2014, **5**, 4670.
4 M. S. Long, A. S. Cans and C. D. Keating, *J. Am. Chem. Soc.*, 2008, **130**, 756–762.
5 A. S. Utada, E. Lorenceau, D. R. Link, P. D. Kaplan, H. A. Stone and D. A. Weitz, *Science*, 2005, **308**, 537–541.
6 A. R. Thiam, R. V. Farese, Jr. and T. C. Walther, *Nat. Rev. Mol. Cell Biol.*, 2013, **14**, 775–786.
7 V. Mikulcová, R. Bordes, A. Minařík and V. Kašpárková, *Food Hydrocolloids*, 2018, **80**, 60–67.
8 B. P. Binks, *Langmuir*, 2017, **33**, 6947–6963.
9 S. Tao, H. Jiang, R. Wang, C. Yang, Y. Li and T. Ngai, *Chem. Commun.*, 2020, **56**, 14011–14014.
10 Y. Qiao, M. Li, D. Qiu and S. Mann, *Angew. Chem., Int. Ed.*, 2019, **58**, 17758–17763.
11 Y. Song, T. C. T. Michaels, Q. Ma, Z. Liu, H. Yuan, S. Takayama, T. P. J. Knowles and H. C. Shum, *Nat. Commun.*, 2018, **9**, 2110.
12 Y. Yin, L. Niu, X. Zhu, M. Zhao, Z. Zhang, S. Mann and D. Liang, *Nat. Commun.*, 2016, **7**, 10658.
13 M. Andes-Koback and C. D. Keating, *J. Am. Chem. Soc.*, 2011, **133**, 9545–9555.
14 Y. Sakuma and M. Imai, *Life (Basel)*, 2015, **5**, 651–675.
15 T. Baumgart, S. T. Hess and W. W. Webb, *Nature*, 2003, **425**, 821–824.
16 D. Gaur, N. C. Dubey and B. P. Tripathi, *Adv. Colloid Interface Sci.*, 2022, **299**, 102566.
17 W. Guo, A. B. Kinghorn, Y. Zhang, Q. Li, A. D. Poonam, J. A. Tanner and H. C. Shum, *Nat. Commun.*, 2021, **12**, 3194.
18 S. Deshpande, W. K. Spoelstra, M. van Doorn, J. Kerssemakers and C. Dekker, *ACS Nano*, 2018, **12**, 2560–2568.
19 K. Kurihara, M. Tamura, K. Shohda, T. Toyota, K. Suzuki and T. Sugawara, *Nat. Chem.*, 2011, **3**, 775–781.
20 F. Walton and K. Wynne, *Nat. Chem.*, 2018, **10**, 506–510.
21 T. Banno, Y. Tanaka, K. Asakura and T. Toyota, *Langmuir*, 2016, **32**, 9591–9597.
22 B. P. Bastakoti and J. Perez-Mercader, *Adv. Mater.*, 2017, **29**, 1704368.
23 L. C. Johnson and R. N. Zia, *Soft Matter*, 2021, **17**, 3784–3797.
24 M. Li, X. Huang and S. Mann, *Small*, 2014, **10**, 3291–3298.
25 F. Lesmes, D. Hochberg, F. Moran and J. Perez-Mercader, *Phys. Rev. Lett.*, 2003, **91**, 238301.
26 S. S. a. B. Zeks, *Int. J. Dev. Biol.*, 1991, **35**, 359–365.
27 L. Giomi and A. DeSimone, *Phys. Rev. Lett.*, 2014, **112**, 147802.
28 J. Man, S. Chien, S. Liang, J. Li and H. Chen, *ChemPhysChem*, 2018, **19**, 1995–1998.
29 H. Seo, C. Nam, E. Kim, J. Son and H. Lee, *ACS Appl. Mater. Interfaces*, 2020, **12**, 55467–55475.
30 T. C. Le and D. A. Winkler, *Chem. Rev.*, 2016, **116**, 6107–6132.
31 L. A. Bawazer, C. S. McNally, C. J. Empson, W. J. Marchant, T. P. Comyn, X. Niu, S. Cho, M. J. McPherson, B. P. Binks, A. deMello and F. C. Meldrum, *Sci. Adv.*, 2016, **2**, e1600567.
32 L. D. Zarzar, V. Sresht, E. M. Sletten, J. A. Kalow, D. Blankschtein and T. M. Swager, *Nature*, 2015, **518**, 520–524.
33 S. R. Liber, O. Marin, A. V. Butenko, R. Ron, L. Shool, A. Salomon, M. Deutsch and E. Sloutskin, *J. Am. Chem. Soc.*, 2020, **142**, 8672–8678.
34 T. G. S. Pushpito and K. Ghosh, *J. Am. Chem. Soc.*, 1980, **102**, 5543–5549.
35 Y. Hu and J. Perez-Mercader, *Macromol. Rapid Commun.*, 2017, **38**, 1600577.
36 Z. Fang, S. Keinan, L. Alibabaei, H. Luo, A. Ito and T. J. Meyer, *Angew. Chem., Int. Ed.*, 2014, **53**, 4872–4876.
37 I. Berlanga, *Biomolecules*, 2019, **9**, 352.
38 R. Tamate, T. Ueki, M. Shibayama and R. Yoshida, *Angew. Chem., Int. Ed.*, 2014, **53**, 11248–11252.
39 Y. Zhang, N. Zhou, N. Li, M. Sun, D. Kim, S. Fraden, I. R. Epstein and B. Xu, *J. Am. Chem. Soc.*, 2014, **136**, 7341–7347.
40 M. Chen, L. Zhou, Y. Guan and Y. Zhang, *Angew. Chem., Int. Ed.*, 2013, **52**, 9961–9965.
41 Y. Onuki, M. Hoshi, H. Okabe, M. Fujikawa, M. Morishita and K. Takayama, *J. Controlled Release*, 2005, **108**, 331–340.
42 W. Wang, A. H. Milani, Z. Cui, M. Zhu and B. R. Saunders, *Langmuir*, 2017, **33**, 8192–8200.
43 Y. Hu and J. Pérez-Mercader, *ACS Appl. Nano Mater.*, 2018, **1**, 3346–3354.
44 A. Kumar, S. Li, C. M. Cheng and D. Lee, *Lab Chip*, 2016, **16**, 4173–4180.
45 L.-Y. C. A. S. Utada, A. Fernandez-Nieves, D. R. Link, C. Holtze and D. A. Weitz, *MRS Bull.*, 2007, **32**, 702–708.
46 V. P. P. B. Umbanhowar and D. A. Weitz, *Langmuir*, 2000, **16**, 347–351.
47 B. Pathak, S. Hatte and S. Basu, *Langmuir*, 2017, **33**, 14123–14129.
48 H. Sadafi, R. Rabani, S. Dehaeck, H. Machrafi, B. Haut, P. Dauby and P. Colinet, *Colloids Surf., A*, 2020, **602**, 125052.
49 P. Zhu, T. Kong, C. Zhou, L. Lei and L. Wang, *Small Methods*, 2018, **2**, 1800017.
50 W. Shi, J. E. Didier, D. E. Ingber and D. A. Weitz, *ACS Appl. Mater. Interfaces*, 2018, **10**, 31865–31869.
51 S. Y. Misyura, *Sci. Rep.*, 2017, **7**, 14759.
52 H. J. Holterman, *Kinetics and evaporation of water drops in air*, Wageningen, The Netherlands, 2003.
53 J. Thiele, V. Chokkalingam, S. H. Ma, D. A. Wilson and W. T. S. Huck, *Mater. Horiz.*, 2014, **1**, 96–101.
54 S. Gsell and M. Merkel, *Soft Matter*, 2022, **18**, 2672–2683.
55 A. F. Routh and B. Vincent, *Langmuir*, 2002, **18**, 5366–5369.
56 Y. Hu and J. Perez-Mercader, *Macromol. Rapid Commun.*, 2017, **38**, 1600577.
57 E. M. Hotze, T. Phenrat and G. V. Lowry, *J. Environ. Qual.*, 2010, **39**, 1909–1924.
58 T. F. Tadros, *Colloids Interface Sci. Ser.*, 2007, **1**, 1–254.
59 T. Lu and E. Spruijt, *J. Am. Chem. Soc.*, 2020, **142**, 2905–2914.

60 R. C. Hayward, A. S. Utada, N. Dan and D. A. Weitz, *Langmuir*, 2006, **22**, 4457–4461.
61 M. Vis, V. F. Peters, E. M. Blokhuis, H. N. Lekkerkerker, B. H. Erne and R. H. Tromp, *Phys. Rev. Lett.*, 2015, **115**, 078303.
62 J. Ryden and P.-A. Albertsson, *J. Colloid Interface Sci.*, 1971, **37**, 219–222.
63 N. Denkov, S. Tcholakova, I. Lesov, D. Cholakova and S. K. Smoukov, *Nature*, 2015, **528**, 392–395.
64 I. Lesov, Z. Valkova, E. Vassileva, G. S. Georgiev, K. Ruseva, M. Simeonov, S. Tcholakova, N. D. Denkov and S. K. Smoukov, *Macromolecules*, 2018, **51**, 7456–7462.
65 R. Iqbal, A. Matsumoto, D. Carlson, K. T. Peters, R. Funari, A. K. Sen and A. Q. Shen, *J. Colloid Interface Sci.*, 2022, **623**, 927–937.